Favorable Concurrence of Static and Dynamic Phenomena at the Morphotropic Phase Boundary of xBiNi$_{0.5}$Zr$_{0.5}$O$_3$-(1-x)PbTiO$_3$

K. Datta,[1,*] R. B. Neder,[2] J. Chen,[3] J. C. Neuefeind,[4] and B. Mihailova[1,†]

[1]*Department of Earth Sciences, University of Hamburg, Hamburg 20146, Germany*
[2]*Department of Crystallography and Structure Physics, Friedrich-Alexander-Universität Erlangen-Nürnberg, Staudtstraße 3, Erlangen 91058, Germany*
[3]*School of Metallurgical and Ecological Engineering, University of Science and Technology Beijing, Beijing 100083, China*
[4]*Chemical and Engineering Materials Division, Oak Ridge National Laboratory, Oak Ridge, Tennessee 37831, USA*

We reveal that concurrent events of inherent entropy boosting and increased synchronization between A- and B-site cation vibrations of an ABO_3-type perovskite structure give rise to a larger piezoelectric response in a ferroelectric system at its morphotropic phase boundary (MPB). It is further evident that the superior piezoelectric properties of xBiNi$_{0.5}$Zr$_{0.5}$O$_3$-(1-x)PbTiO$_3$ in comparison to xBiNi$_{0.5}$Ti$_{0.5}$O$_3$-(1-x)PbTiO$_3$ are due to the absolute flattening of the local potentials for all ferroelectrically active cations with a higher spontaneous polarization at the MPB. These distinctive features are discovered from the analyses of neutron pair distribution functions and Raman scattering data at ambient conditions, which are particularly sensitive to mesoscopic-scale structural correlations. Altogether this uncovers more fundamental structure-property connections for ferroelectric systems exhibiting a MPB, and thereby has a critical impact in contriving efficient novel materials.

Perovskite-based ferroelectric materials are an important class of functional materials and a key topic in materials science. One of the major challenges in this field is to build rigorous and generic structure-property relationships to better understand the morphotropic phase boundary (MPB) where physical properties are enhanced anomalously. The manifestation of superior properties on the onset of a MPB has been broadly discussed so far in the light of structure and thermodynamics as the existence of low-symmetry phases and the overall flattening of the free energy surfaces or structural instabilities, respectively, which facilitate the polarization rotation under external stimuli [1–5]. However, these prevailing concepts cannot fully identify the distinctive system-dependent atomistic mechanism in order to explain the comparative behavior—a key ingredient for developing efficient and benign materials. The complexity of this problem arises from the existence of multiple competing structural correlations, such as chemical order, correlated displacement, octahedral tilts, and different types of bonding in a multicomponent ferroic system, whose distinct characterization in a quantitative or qualitative manner is often very subtle [6–8]. Although there have been many recent experimental attempts to build more convincing structural models mimicking the atomic-level structural correlations in complex systems [9–17], the challenge in formulating a robust atomistic model still exists.

In this context, we have applied total neutron scattering and Ramam scattering methods to two promising ferroeletric solid solutions, xBiNi$_{0.5}$Ti$_{0.5}$O$_3$-(1-x)PbTiO$_3$ (xBNT-PT) and xBiNi$_{0.5}$Zr$_{0.5}$O$_3$-(1-x)PbTiO$_3$ (xBNZ-PT), in order to establish structure-property connections based on atomic-level information.

Perovskite-based ferroelectric systems with the general formula xBiMeO$_3$-(1-x)PbTiO$_3$ have become hugely popular lately because of their excellent physical properties with a broader range of operating temperatures, and moreover due to their reduced Pb content in comparison to PbZr$_x$Ti$_{1-x}$O$_3$, which has been the material of choice for the last four decades. In particular, xBNZ-PT has attracted a lot of attention because of its unusually high piezoelectric coefficients at $x_{MPB} = 0.40$ relative to its parent system xBNT-PT ($d_{33} \sim 400$ and 260 pC/N, respectively) [18,19]. It has the further advantage of being inexpensive because of the raw materials compared to BiScO$_3$-PbTiO$_3$ [20] and BiNi$_{0.5}$Hf$_{0.5}$O$_3$-PbTiO$_3$ [21]. Therefore, it is considered a promising candidate to replace the currently used piezoelectric materials [22].

In this Letter, we focus on the key question: Why does xBNZ-PT demonstrate better piezoelectric properties than xBNT-PT at the MPB? In doing so, we reveal how the incorporation of Zr^{4+} at the B sublattice influences the structural disorder at the mesoscopic scale and subsequently, combined with the cooperative A- and B-site atomic vibrations, generates favorable conditions for better piezoelectric properties. The discovered local structural features in general provide a new approach to develop more inclusive structure-property relations in ferroelectric solid solutions with MPBs.

Room temperature neutron powder diffraction experiments on xBNT-PT and xBNZ-PT ceramics—produced by a typical solid state synthesis method [18,23]—were carried out at the NOMAD beam line at Oak Ridge National
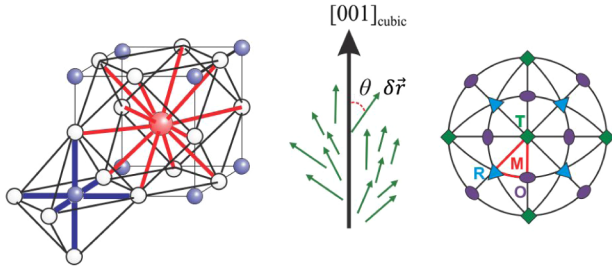
FIG. 1. Schematics of an aristotype perovskite structure showing the 12 and six oxygen neighbors of the A-site (red) and B-site (blue) cation, respectively. On the right is a typical $[001]_{cubic}$ stereograph onto which the directions of the polar displacements ($\delta\vec{r}$) have been mapped.

Laboratory (ORNL). Pair distribution functions (PDFs) were obtained through running a data-correction procedure followed by the Fourier transformations with a maximum reciprocal-space vector Q of 31.4 Å^{-1}. The modelings of the PDFs were done using the RMCPROFILE package, which performs typical big-box modeling implementing the reverse Monte Carlo (RMC) technique [24,25]. Analyses of the RMC-refined structural models were done using the various tools available as part of the DISCUS software [26]. Complementary room-temperature Raman scattering data as a function of composition were collected with a Horiba Jobin-Ivon T64000 triple-grating spectrometer providing a spectral resolution of 2 cm^{-1} and a peak-position precision of 0.35 cm^{-1}. More details on the experiments and analyses are given in the Supplemental Material [27].

Given the fact that most of the technological interests in ferroelectric materials including their piezoelectric and dielectric properties are governed by their spontaneous polarization, we have examined the inherent polar displacements $\delta\vec{r}$ of the cations calculated with respect to the center of their corresponding oxygen environment, as schematically shown in Fig. 1 [6,15,16,28]. The distributions of the magnitudes $|\delta\vec{r}|$ and the directions $\delta\hat{r}$ of the displacements were extracted from the RMC-refined structural models.

Figure 2 shows the development of such direction distributions as a function of composition for both xBNT-PT and xBNZ-PT, where the directions are mapped onto the standard $[001]_{pc}$ (pc refers to pseudocubic setting) stereograph. Primarily, the maps depict the evolution of the statistical trend of $\delta\hat{r}$ with the composition reflecting the long-range or the Bragg symmetry of the system. However, beyond that, the maps virtually describe the local correlations of the polar displacements in terms of their ordering, or, in other words, the variations of the local polarization directions within the system in its virgin state. Hence, one can also relate these graphs to the atomic-scale order-disorder characteristics, from which it is possible to envisage the development of the local potential surfaces of each cation with x.

In order to quantify the observed statistical information of $\delta\hat{r}$, we have calculated the so-called orientational order paramerter $S = 1.5\langle\cos^2\theta\rangle - 0.5$ (see Fig. 3), where θ is the angle between $[001]_{pc}$ and $\delta\vec{r}$. The parameter S simply signifies the extent of randomness in the directions when the distributions are more or less symmetric around the chosen director, which is $[001]_{pc}$ here. Therefore, it is evident that as x increases, both systems exhibit a gradual increase in disorder characterized by the stochasticity of the intrinsic polar order. Notably, xBNZ-PT differs from xBNT-PT by the fact that both A- and B-site cations have a similar level of randomness (comparable S values), while in xBNT-PT, the B-site cations show a higher level of disorder (lower S values) than the A-site cations in the range $0.20 \leq x \leq x_{MPB}$. This indicates that the isovalent substitution of Zr^{4+} significantly affects the ferroic order of the A-site cations—presumably through the enhanced local elastic stress caused by the larger ionic radius of Zr^{4+}, which subsequently shifts the MPB to a lower value of x compared to that of xBNT-PT.

It is interesting to see that the MPB of xBNT-PT and xBNZ-PT at $x = 0.55$ and 0.40, respectively, can be straightaway told apart from the development of the $\{002\}_{pc}$ Bragg peak [Fig. 2(a)], but the short-range neutron PDFs (Fig. S2 of Ref. [27]) exhibit a gradual change with
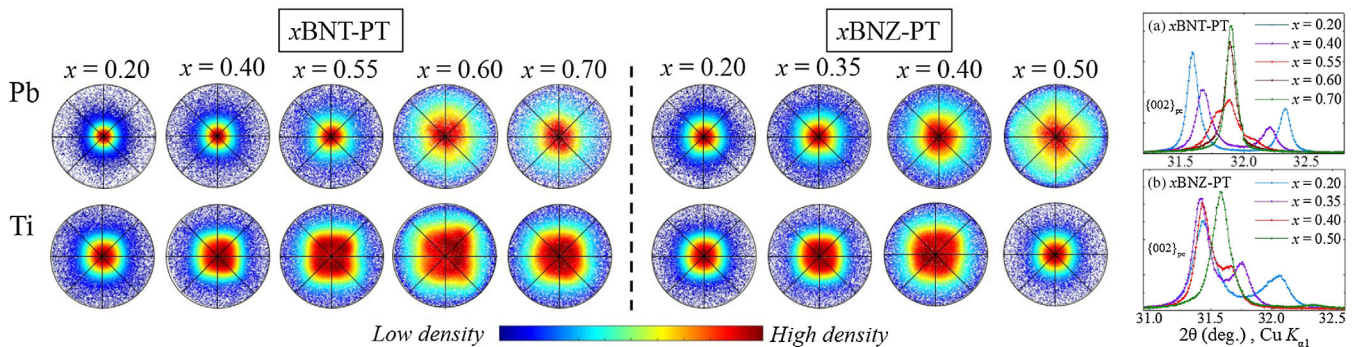
FIG. 2. Stereographs of the directions ($\delta\hat{r}$) of polar displacements as obtained from the refined structural models as a function of composition. The colors exhibit the density distribution around each point on the graph and therefore help to classify the statistical trends in terms of their symmetry. On the right, the development of $\{002\}_{pc}$ Bragg reflections are shown for both compounds obtained from the laboratory x-ray diffraction experiments. The stereographs of the other A- and B-site cations as a function of composition are included in Supplemental Material (Fig. S4) [27].
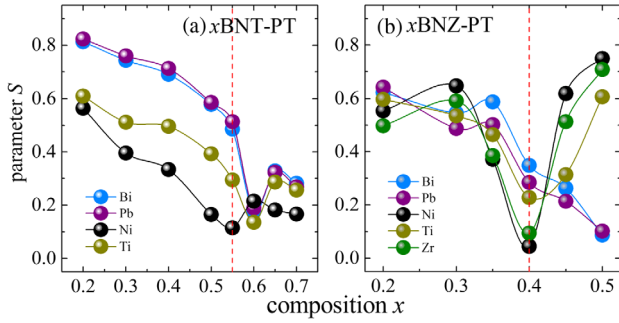
FIG. 3.   Development of the parameter S for A- and B-site cations as a function composition for both solid solutions.

increasing x. Therefore, together with the stereographs, it provides direct evidence that the composition-directed phase transformations are more of an order-disorder type than a displacive type, which is generally considered a signature feature of ferroelectric solid solutions with MPBs. In addition, we have not detected any chemical ordering at A- or B-site cation sublattices in our refined models for both cases (Fig. S6 of Ref. [27]), defying some reported assumptions based on the theoretical calculations on analogous systems [29,30]. The stereographs of xBNT-PT also point out that the A-site cations maintain a strong $[001]_{\text{pc}}$-type directional preference at the MPB, while in xBNZ-PT both A- and B-site cations simultaneously exhibit a pronounced dispersion of $\delta\hat{r}$ at $x = x_{\text{MPB}}$. The prominent $[001]_{\text{pc}}$ propensity for the A-site cation displacements in xBNT-PT in fact nicely complements the recent study that detected substantial inherent tetragonal domain alignment before poling [31].

Figure 4 demonstrates the variations of $|\delta\vec{r}|_{\text{mean}}$ along with their standard deviations ($\sigma(|\delta\vec{r}|)$) as a function of x, which were estimated from the histograms of the magnitudes of the polar shifts (Fig. S7 of Ref. [27]). It is evident that the addition of larger Zr^{4+} ($r_{\text{ionic}} = 0.78$ Å) induces greater shifts for the A-site cations as well as larger standard deviations [Figs. 4(c) and 4(d)]. Importantly though, in both systems the A-site cation displacements remain

relatively constant with x (average $|\delta\vec{r}|_{\text{mean}} = 0.40$ and 0.45 Å for xBNT-PT and xBNZ-PT, respectively), whereas the B-site cations in xBNZ-PT show a decrease in $|\delta\vec{r}|_{\text{mean}}$ upon approaching the MPB from $x = 0.20$, justifying the fact that Pb-based ferroelectrics are predominantly A-site driven ferroelectrics [32,33].

So far it appears that the superior piezoelectric properties of xBNZ-PT at the MPB are stemming from the higher structural disorder characterized by local random ferroelectric order together with the increased A-site cation shifts with respect to that of xBNT-PT. However, this cannot explain the drop in the piezoelectric coefficient just above or below the exact MPB composition in both systems (Fig. 5). For instance, xBNT-PT does not render better piezoelectric properties at $x = 0.60$ where the cations exhibit very similar values of $|\delta\vec{r}|_{\text{mean}}$ including the highest orientational disorder of the shifts. Therefore, considering the above facts one can draw out a few inferences: the gross enhancement phenomenon for a particular system is thoroughly driven by the so-called extrinsic contributors as the combined variation of $|\delta\vec{r}|$ cannot account for the observed enhancement at $x = x_{\text{MPB}}$. Second, the exact or the relative values of the piezoelectric properties cannot be fully anticipated considering solely the concepts based on ferroelectric instabilities. They may well be a necessary factor but they are surely not sufficient in order to deliver the amplification at the MPBs, because equilibrium atomic configurations with different compositions exhibiting similar disorder differ significantly in their properties (Fig. 5).

The quest for a more comprehensive answer to the above puzzle led us to investigate the room-temperature Raman scattering data in order to gather complementary information related to the atomic dynamics. The deconvolution of the Raman spectra through a rigorous peak-fitting procedure helps us to follow the development of distinctive A- and B-site cation vibrations as a function of composition. The respective peaks were categorized following the previously reported assignments [17,35–37]. Figure 6 shows the development of two deduced factors typically considered for a two-component behavior: (1) the average of the squared
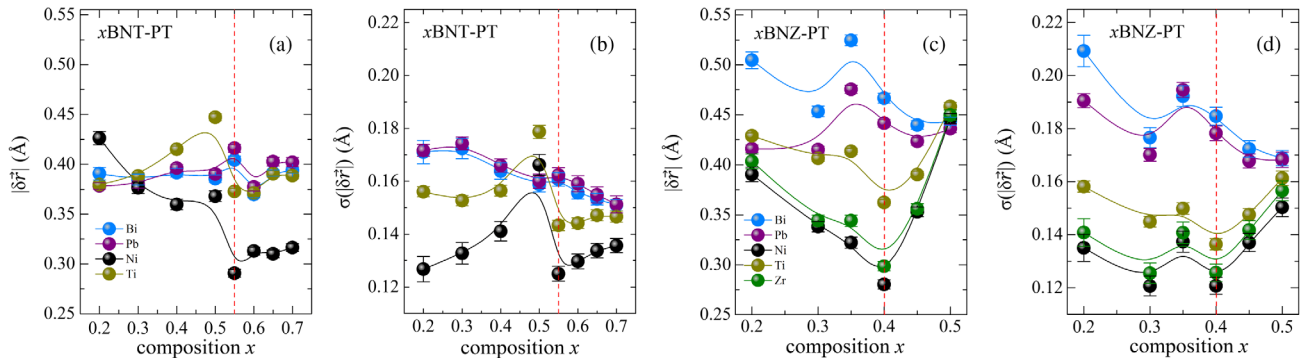
FIG. 4.   Mean displacements ($|\delta\vec{r}|_{\text{mean}}$) and their standard deviations [$\sigma(|\delta\vec{r}|)$] as a function of composition for both solid solutions. The histograms of the magnitudes ($|\delta\vec{r}|$) can be found in Fig. S7 of the Supplemental Material [27]. The histograms of the magnitudes conform to the direction trends as shown in Fig. 1 (Fig. S5 of Ref. [27]), meaning that $|\delta\vec{r}|_{\text{mean}}$ can be used as the characteristic parameter of the system. The solid lines in the plots are only guides to the eye.
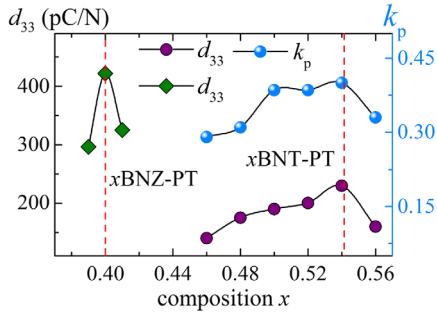
FIG. 5.   Reported piezoelectric properties for (a) xBNT-PT and (b) xBNZ-PT ceramic samples, taken from Refs. [18,34], respectively.

wave numbers $\langle\omega\rangle = \sqrt{(\omega_i^2 + \omega_j^2)/2}$, and (2) the normalized difference $\Delta\omega = [(\omega_i^2 - \omega_j^2)/2(\omega_i^2 + \omega_j^2)]$, which reveal specific similarities and differences in the overall characteristics of the two systems. $\langle\omega\rangle$ reflects the average dynamic energy state of a given type of atom, while $\Delta\omega$ represents the energy difference between the distinct dynamic states and thereby describes the local structural anisotropy. Evidently, the $\langle\omega_A\rangle$ involving mainly A-site cation vibrations (ω_1 and ω_2 in Fig. S9 of Ref. [27]) demonstrate a prominent softening at the MPB [Fig. 6(a)]. However, the softening in the case of xBNZ-PT is much stronger than that in xBNT-PT. The development of $\Delta\omega$ illustrates another important difference in the thermodynamic picture between the two systems: A-site cations in xBNZ-PT experience complete flattening ($\Delta\omega_A = 0$) in their local potential at the MPB, whereas in xBNT-PT there are still distinguishable energy states with diminished energy barriers as $\Delta\omega_A$ remains nonzero throughout the composition range [Fig. 6(a), inset].

On the other hand, the B-site cations exhibit gradual hardening of $\langle\omega\rangle_B$ in xBNT-PT with increasing x [inset of Fig. 6(c)], whereas $\langle\omega\rangle_B$ softens at the MPB for xBNZ-PT. Nevertheless, the two components of the B-site cations eventually merge into a single peak at the MPB in both cases [$\Delta\omega_B = 0$ in Fig. 6(c)] and reveal the concomitant flattening of the corresponding local potential surfaces.

Nevertheless, the most interesting feature from the Raman scattering data can be pointed out from Fig. 6(b), which displays the softening of the A-BO_3 phonon mode (ω_3) at the MPBs of both systems. This mode comprises the vibrations of both A- and B-site cations corresponding to a T_{1u} phonon in the aristotype $Pm\bar{3}m$ structure [35]. Such a softening as a distinctive phenomenon has been also detected in xBiMg$_{0.5}$Ti$_{0.5}$O$_3$-(1-x)PbTiO$_3$ [17] and (1-x)Na$_{0.5}$Bi$_{0.5}$TiO$_3$-xBaTiO$_3$ [36]. Hence, the ubiquitousness of this increased dynamic coupling between A- and B-site cations occurring precisely at the MPBs provides a new perspective based on the dynamics of the atomic vibration to identify the critical point as a MPB in a phase diagram where significant enhancement of the properties can be achieved.

Altogether, it suffices to say that the anomalous enhancement of the piezoelectric properties in xBNZ-PT with respect to xBNT-PT is an overall effect of the complete flattening of
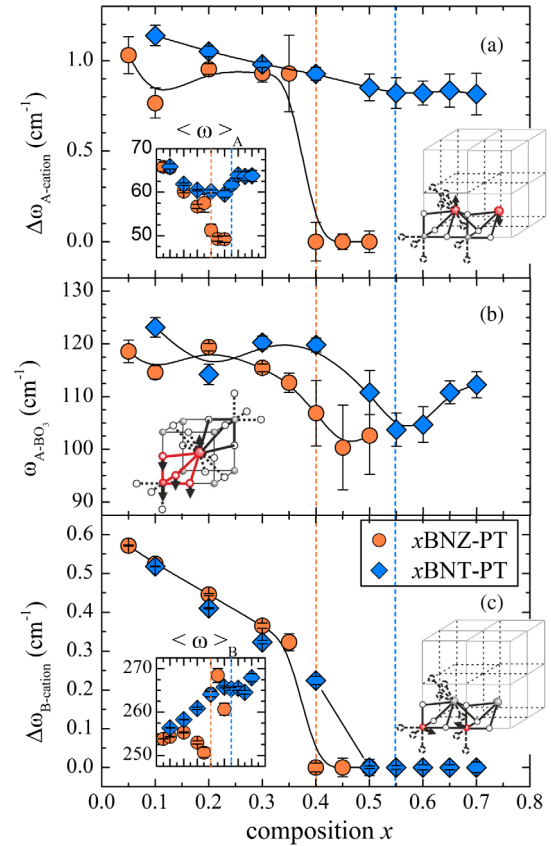
FIG. 6.   Development of the $\Delta\omega$ and $\langle\omega\rangle$ parameters comprising discrete vibrations of A-site cations (a), B-site cations (c), and the phonon mode ω_3 (b) involving both A- and B-site cations. The solid lines in the plots are simply guides to the eye. The overall Raman spectra as a function of composition for both systems can be found in Fig. S8 of Ref. [27]. The sketches represent the atomic vibrations of the corresponding cubic phonon modes.

the free energy surfaces for all cations occurring together with the strong dynamic coupling between the A- and B-site cations at the MPB. Naturally, these results have general implications in classifying the roles of the different atomistic mechanisms that drive the properties at a MPB. The current results together with our earlier reports on other ferroelectric solid solutions [17,36] show unequivocally that the softening of the A-BO_3 phonon mode is an indispensable event occurring exactly at the MPB and therefore strongly suggest that this coupling has a major role in determining the properties. However, the flattening of the local-potential surfaces is necessary in order to maximize the effect of property enhancement. The exact relative enhancement would also depend on the structural polarity ($|\vec{\delta r}|_{\rm mean}$), and this is probably why the Pb-based systems, where Pb^{2+} seems to maintain steady and large values of local distortion irrespective of the chemical substitutions [8], exhibit superior properties compared to the Pb-free systems, including better thermal stability. Inevitably, the full or partial absence of any of the mentioned phenomena will not give rise to the maximum increase in the properties.

Generally speaking, our results have unraveled local structural correlations extending up to a few unit cells that are responsible for the MPB properties of ferroelectric solid solutions, which essentially enrich the established concept related to the rotation of the polarization in a strain-reduced environment. We can now say that the mere existence of a low-symmetry phase(s) and/or structural instability facilitating polarization rotation will not ensure the greatest MPB properties, unless the pivotal alliance occurs between the atomic vibrations and the flattening of the free-energy surfaces for all constituent cations. Besides, it is equally important that the system should retain or obtain higher values of inherent structural polarity.

The above atomistic features of a composition-induced phase transition not only expose more fundamental structure-property connections based on static and dynamic information, but more importantly invoke the fingerprinting of MPBs where strong amplification of the piezoelectric properties can be accomplished. As such, this helps us to classify seemingly similar MPBs with varied level of performances and above all provides directions for the improvements. Therefore, in terms of either contriving new materials or tweaking the properties, one should consider more of the chemical aspects of the individual elements and their influence on the structure at the mesoscopic scale instead of the changes in the average structure. We presume that simultaneous substitutions on A and B sites with a large elastic mismatch would be helpful to develop essential effects—static and dynamic—in order to bring about the best properties.

---

[*]kaustuv.datta@uni-hamburg.de

[†]boriana.mihailova@uni-hamburg.de

[1] H. Fu and R. Cohen, Nature (London) **403**, 281 (2000).

[2] B. Noheda, D. E. Cox, G. Shirane, S. E. Park, L. E. Cross, and Z. Zhong, Phys. Rev. Lett. **86**, 3891 (2001).

[3] M. Ahart, M. Somayazulu, R. E. Cohen, P. Ganesh, P. Dera, H. Mao, R. Hemley, Y. Ren, P. Liermann, and Z. Wu, Nature (London) **451**, 545 (2008).

[4] D. Damjanovic, J. Am. Ceram. Soc. **88**, 2663 (2005).

[5] M. Budimir, D. Damjanovic, and N. Setter, Phys. Rev. B **73**, 174106 (2006).

[6] I. Grinberg, V. Cooper, and A. Rappe, Nature (London) **419**, 909 (2002).

[7] I. Grinberg and A. M. Rappe, Phys. Rev. B **70**, 220101(R) (2004).

[8] T. Egami, Annu. Rev. Mater. Res. **37**, 297 (2007).

[9] Y. M. Jin, Y. U. Wang, G. Khachaturyan, J. F. Li., and D. Viehland, Phys. Rev. Lett. **91**, 197601 (2003).

[10] T. Egami, Struct. Bond. **124**, 69 (2007).

[11] W. Dmowski, S. B. Vakhrushev, I.-K. Jeong, M. P. Hehlen, F. Trouw, and T. Egami, Phys. Rev. Lett. **100**, 137602 (2008).

[12] R. G. Burkovsky, Y. A. Bronwald, A. V. Filimonov, A. I. Rudskoy, D. Chernyshov, A. Bosak, J. Hlinka, X. Long, Z.-G. Ye, and S. B. Vakhrushev, Phys. Rev. Lett. **109**, 097603 (2012).

[13] H. Takenaka, I. Grinberg, and A. M. Rappe, Phys. Rev. Lett. **110**, 147602 (2013).

[14] W. Ge, C. P. Devreugd, D. Phelan, Q. Zhang, M. Ahart, J. Li, H. Luo, L. A. Boatner, D. Viehland, and P. M. Gehring, Phys. Rev. B **88**, 174115 (2013).

[15] N. Zhang, H. Yokota, A. M. Glazer, Z. Ren, D. A. Keen, D. S. Keeble, P. A. Thomas, and Z.-G. Ye, Nat. Commun. **5**, 5231 (2014).

[16] K. Datta, A. Richter, M. Göbbels, D. A. Keen, and R. B. Neder, Phys. Rev. B **93**, 064102 (2016).

[17] K. Datta, R. B. Neder, J. Chen, J. C. Neuefeind, and B. Mihailova, Sci. Rep. **7**, 471 (2017).

[18] Y. Rong, J. Chen, H. Kang, L. Liu, L. Fang, L. Fan, Z. Pan, and X. Xing, J. Am. Ceram. Soc. **96**, 1035 (2013).

[19] S. M. Choi, C. J. Stringer, T. R. Shrout, and C. A. Randall, J. Appl. Phys. **98**, 034108 (2005).

[20] R. Eitel, C. Randall, T. Shrout, P. Rehrig, W. Hackenberger, and S.-E. Park, Jpn. J. Appl. Phys. **40**, 5999 (2001).

[21] Z. Pan, J. Chen, L. Fan, L. Liu, L. Fang, and X. Xing, J. Appl. Phys. **112**, 114120 (2012).

[22] Z. Xie, Z. Yue, G. Ruehl, B. Peng, J. Zhang, Q. Yu, X. Zhang, and L. Li, Appl. Phys. Lett. **104**, 243902 (2014).

[23] P. Hu, J. Chen, J. Deng, and X. Xing, J. Am. Chem. Soc. **132**, 1925 (2010).

[24] M. G. Tucker, M. T. Dove, and D. A. Keen, J. Appl. Crystallogr. **34**, 630 (2001).

[25] R. L. McGreevy, J. Phys. Condens. Matter **13**, R877 (2001).

[26] R. B. Neder and T. Proffen, *Diffuse Scattering and Defect Structure Simulations—A Cook Book Using the Program* DISCUS (Oxford University Press, New York, 2007).

[27] See Supplemental Material at http://link.aps.org/supplemental/10.1103/PhysRevLett.119.207604 for additional figures and more details on the adopted methodology for the data analyses.

[28] D. S. Keeble, E. R. Barney, D. A. Keen, M. G. Tucker, J. Kreisel, and P. A. Thomas, Adv. Funct. Mater. **23**, 185 (2013).

[29] D. D. Khalyavin, A. N. Salak, N. P. Vyshatko, A. B. Lopes, N. M. Olekhnovich, A. V. Pushkarev, I. I. Maroz, and Y. V. Radyush, Chem. Mater. **18**, 5104 (2006).

[30] K. Miura, M. Kubota, M. Azuma, and H. Funakubo, Jpn. J. Appl. Phys. **48**, 09KF05 (2009).

[31] G. Tutuncu, L. Fan, J. Chen, X. Xing, and J. Jones, Appl. Phys. Lett. **104**, 132907 (2014).

[32] J. Shi, I. Grinberg, X. Wang, and A. M. Rappe, Phys. Rev. B **89**, 094105 (2014).

[33] M. Ghita, M. Fornari, D. J. Singh, and S. V. Halilov, Phys. Rev. B **72**, 054114 (2005).

[34] Q. Zhang, M. Jiang, and Z. Li, J. Electroceram. **29**, 179 (2012).

[35] A.-M. Welsch, B. J. Maier, B. Mihailova, R. J. Angel, J. Zhao, C. Paulmann, J. M. Engel, M. Gospodinov, V. Marinova, and U. Bismayer, Z. Kristallogr. **226**, 126 (2011).

[36] K. Datta, A. Richter, M. Göbbels, R. B. Neder, and B. Mihailova, Phys. Rev. B **90**, 064112 (2014).

[37] K. Datta, A. Richter, M. Göbbels, R. B. Neder, and B. Mihailova, Phys. Rev. B **92**, 024107 (2015).